Chemical Science

ROYAL SOCIETY OF CHEMISTRY

EDGE ARTICLE

View Article Online
View Journal | View Issue

Cite this: *Chem. Sci.*, 2026, **17**, 3691

All publication charges for this article have been paid for by the Royal Society of Chemistry

Received 11th November 2025
Accepted 14th December 2025

DOI: 10.1039/d5sc08753h

rsc.li/chemical-science

Guest-induced emission enhancement in the permanent porous conjugated carboracycle crystal

Kazuhiro Yuhara, [a] Sota Takemori,[a] Takumi Yanagihara, [a] Shunsuke Ohtani, [b] Tomoki Ogoshi [bc] and Kazuo Tanaka *[ad]

Macrocyclization can provide space for realizing host–guest-mediated molecular sensing based on the regulation of excited-state structural change. Here, we report guest-induced luminescent changes in crystalline *o*-carborane-containing conjugated macrocycles, which develop an intrinsically porous crystal with 1D channels. The crystal can capture C4-length vaporous guests and subsequently exhibit guest-induced emission enhancement through the suppression of excited-state structural relaxation. Notably, the crystal showed successful reversible guest encapsulation without losing its crystalline porosity, as well as heat resistance up to 500 °C.

Introduction

Solid-state emissive molecules with stimuli-responsiveness have attracted tremendous attention as a platform for next-generation optoelectronics.[1] However, the environmental sensitivity of conventional organic luminophores is often spoiled due to aggregation-caused quenching (ACQ). One of the potential strategies for overcoming the problem of ACQ is the employment of aggregation-induced emission (AIE)-active molecules (AIEgens), which exhibit intense emission only in solid states and their intrinsic environment-sensitive optical properties.[2] Previous reports have suggested that the solid-state luminescence properties in AIE should be related to the degree of structural relaxation in the excited state.[3,4] When surrounding molecules tightly restrict the molecular motion of the chromophores in the excited state, the photochemical channels to non-radiative deactivation processes should be closed, resulting in significant emission enhancement.[5] Based on this mechanism, various AIEgens have been extensively studied in terms of their structure–property relationships and applied as imaging probes.[6] Currently, further applications in next-generation smart devices are being explored, and solid-state emissive materials including AIEgens are expected to have more stimuli-responsiveness, *i.e.* luminochromic properties, in response to external stimuli or environmental changes.[7]

As a next research step, the design of external stimuli to control the solid-state luminescence would be of importance. The restriction of molecular motion by aggregation often hinders responses to the surrounding environment, thus decreasing their stimuli-responsiveness and impeding the controllability of their luminescence properties.[8] One promising design strategy to enhance sensitivity toward environmental changes is the introduction of spaces within the molecule. For example, macrocycle-containing AIEgens can provide an internal cavity that can accommodate molecular motion, and the host–guest properties of macrocycles can be a trigger for controlling their solid-state optical properties.[9] To date, many studies have reported AIEgen-based macrocycles,[10] whereas only a few reports have addressed solid-state host–guest properties and their effect on luminescence.

A boron and carbon cluster, *o*-carborane, is known to act as a key unit for constructing functional AIEgens.[11] *C*-Aryl *o*-carborane derivatives typically show intramolecular charge transfer (ICT) emission originating from orbital conjugation between the aryl moiety and the cluster unit (Fig. 1a).[12] The excited-state structures in the ICT states were theoretically studied using the following two structural parameters: the lengths of the carbon–carbon bond in the cluster (C_{cage}–C_{cage} bond) and the dihedral angles between aryl units and the C_{cage}–C_{cage} bond (φ_{Ar-CB}). The ICT state can be formed when the π-plane of the aryl moiety orients perpendicularly to the C_{cage}–C_{cage} bond ($\varphi_{Ar-CB} \sim 90°$), accompanied with significant elongation of the bond from 1.6–1.9 Å in the ground state to 2.2–2.4 Å in the excited state (Fig. 1b left).[13] Furthermore, recent studies suggest that when the aryl moiety aligns parallel to the C_{cage}–C_{cage} bond ($\varphi_{Ar-CB} \sim 0°$) accompanied with its further elongation to ~2.5 Å (Fig. 1b right), a completely charge-separated state, followed by a non-emissive dark state possessing only slight oscillator strength, should be formed.[14,15] These emissive ICT and non-emissive

[a]*Department of Polymer Chemistry, Graduate School of Engineering, Kyoto University, Katsura, Nishikyo-ku, Kyoto 615–8510, Japan. E-mail: tanaka@poly.synchem.kyoto-u.ac.jp*

[b]*Department of Synthetic Chemistry and Biological Chemistry, Graduate School of Engineering, Kyoto University, Katsura, Nishikyo-ku, Kyoto 615–8510, Japan*

[c]*WPI Nano Life Science Institute (WPI-NanoLSI), Kanazawa University, Kakuma-machi, Kanazawa, Ishikawa 920–1192, Japan*

[d]*Department of Technology and Ecology, Graduate School of Global Environmental Studies, Kyoto University, Katsura, Nishikyo-ku, Kyoto 615–8510, Japan*

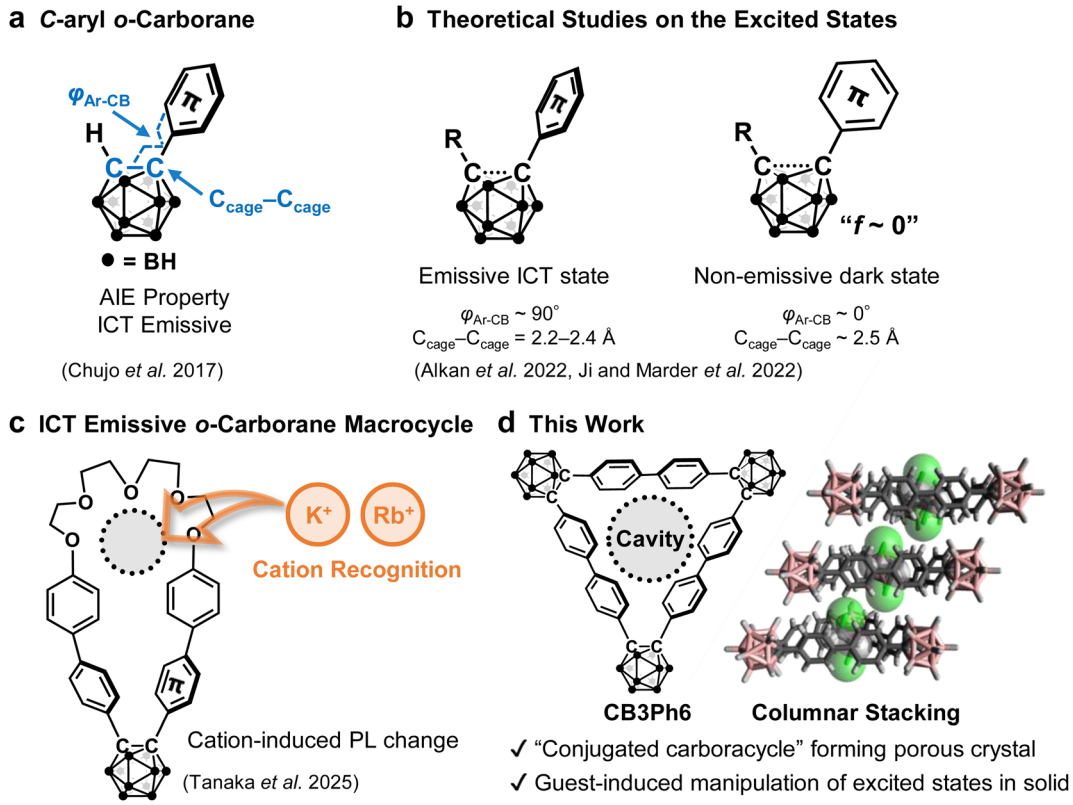

Fig. 1 Reported examples of (a) *C*-aryl *o*-carborane derivatives, (b) theoretical studies on the excited states of derivatives forming ICT states, and (c) an ICT emissive *o*-carborane-based macrocycle. *f* denotes oscillator strength. (d) Chemical structure and crystal-state columnar stacking of **CB3Ph6**, with an overview of this work.

dark states play key competitive roles in photochemistry of *o*-carboranes. As a related example, we previously found that host–guest interaction can regulate excited-state structural relaxation in *o*-carborane-based macrocycles containing pseudo-crown ether (Fig. 1c).[16] The macrocycles showed emission enhancement upon solution-state host–guest complexation due to the suppression of molecular motion, which quenches emission.

There have been a number of C_3-symmetric macrocyclic compounds with precise host–guest chemistry.[17,18] *C*,*C*′-Difunctionalized *o*-carborane can be implemented at the corner of molecular triangles.[19] Herein, we report a macrocycle consisting of cyclo-trimerized diphenyl *o*-carborane (**CB3Ph6**, Fig. 1d) as a conjugated carboracycle.[20] Interestingly, **CB3Ph6** formed a crystal with permanent intrinsic porosity,[21] in which guest-accessible 1D channels were developed through columnar stacking of the macrocycles. Moreover, **CB3Ph6** showed AIE properties, and its porous crystal showed emission enhancement upon encapsulation of vaporous guests. Theoretical calculations suggest that the filling of the cavities by guests should restrict the excited-state structural relaxation, leading to the closing of the channel to the non-emissive dark states. In addition, the crystal showed reversible guest release and capture without changing its crystalline porosity and no chemical decomposition up to 500 °C. To the best of our knowledge, this is the first example of a porous crystal with guest-encapsulation-triggered luminochromic behaviors and superior thermal stability based on the carboracycle molecule.

Results and discussion

Synthesis and crystallization

The macrocycle **CB3Ph6** was successfully synthesized by Ni(0)-mediated trimerization of 1,2-bis(4-bromophenyl)-*o*-carborane[22] (Schemes S1, S2 and Charts S1–S3, S10). The dibrominated precursor was consumed quantitatively under the reaction conditions. Purification was initially performed by column chromatography on SiO_2. After column chromatography, a mixture of the product and other byproducts was still obtained. Recrystallization was then performed with 1,2-dichloroethane (DCE) to afford pure crystalline products. The synthesis of the macrocycle proceeded with a poor isolated yield of 4%, probably due to the formation of a large amount of precipitate, likely an oligomerization or polymerization product. The single-crystal of **CB3Ph6** containing DCE (**DCE@CB3Ph6**) was obtained by vapor diffusion of MeOH into the DCE solution at −30 °C, followed by slow evaporation of the solvent at room temperature. Single-crystal X-ray diffraction (SCXRD) analysis revealed that DCE molecules occupied the cavity of each macrocycle to form a 1 : 1 host–guest complex (Fig. 2a, b, S1 and Table S1). The encapsulated DCE molecules had multiple C–H···π interactions with the biphenyl sides

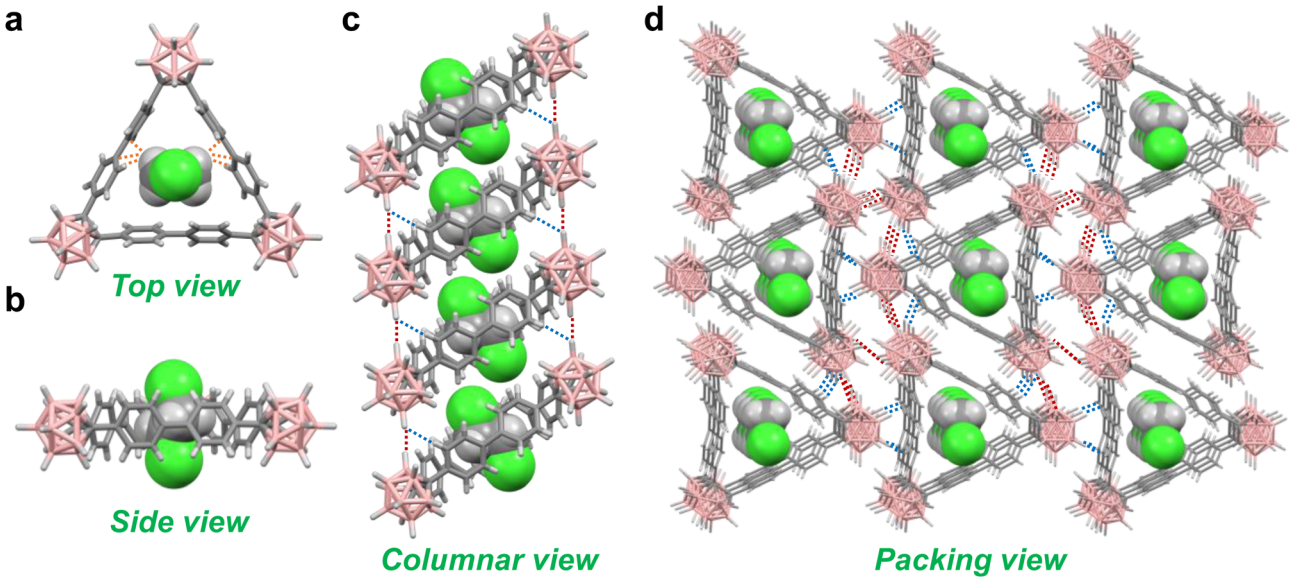

Fig. 2 Single-crystal structures of **DCE@CB3Ph6**: (a) top, (b) side, (c) columnar, and (d) packing views. Orange, red and blue dotted lines indicate C–H···π, B–H···(H–)B, and B–H···H–C contacts (<sum of vdW radii), respectively. Colors: C, gray; B, pink; H, white; Cl, green.

located between *o*-carborane corners. The **CB3Ph6** molecules aligned in a columnar structure with 1D channels (Fig. 2c). The stacked **CB3Ph6** molecules were involved in B–H···H–B and B–H···H–C contacts. The columns assembled to form a packed structure, with several B–H···B, B–H···H–B, and B–H···H–C contacts existing among them (Fig. 2d).

Adsorption and thermal properties

To investigate the effects of solvent inclusion on the physical properties, the guest-free crystal (**CB3Ph6**α) was prepared by heating **DCE@CB3Ph6** at 100 °C under vacuum for 3 h. The removal of DCE was monitored *via* ^{1}H NMR spectroscopy (Chart S4). Unfortunately, a single-crystal sample of **CB3Ph6**α suitable

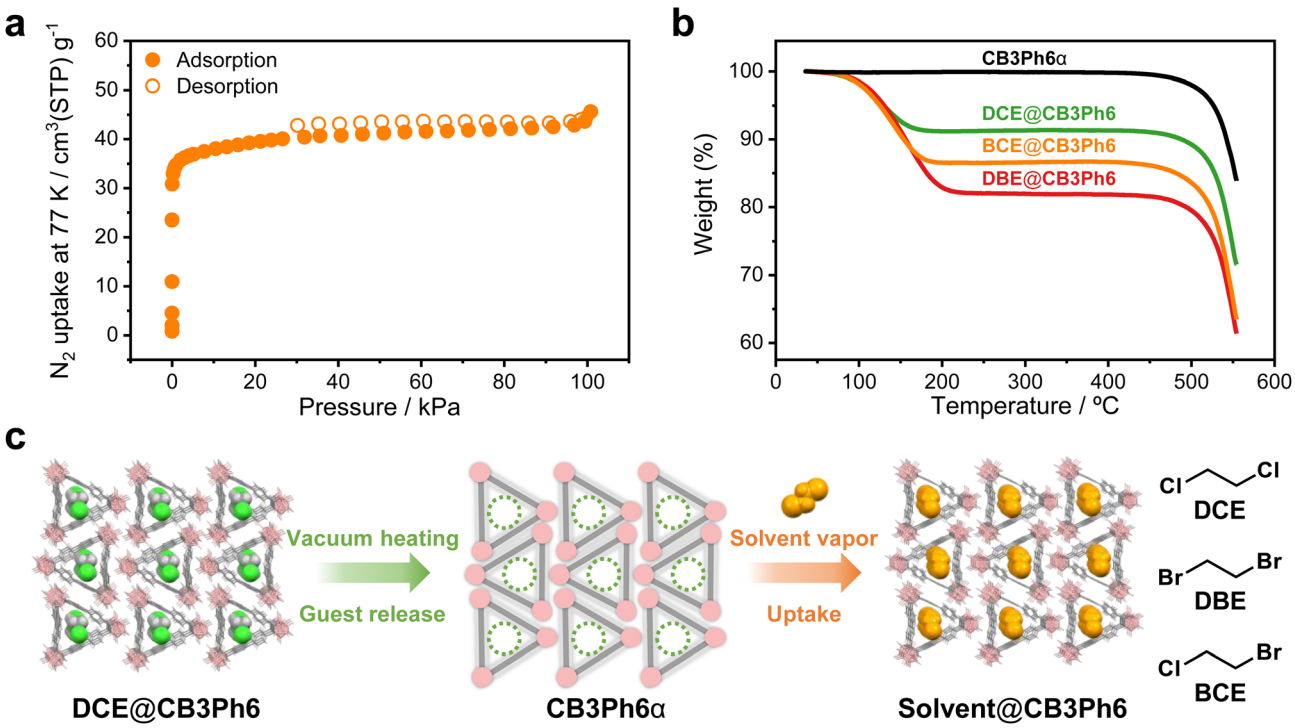

Fig. 3 (a) N_2 sorption isotherm of **CB3Ph6**α recorded at 77 K. Solid and open circles represent adsorption and desorption, respectively. (b) TGA thermograms of **CB3Ph6**α (black), **DCE@CB3Ph6** (green), **DBE@CB3Ph6** (red), and **BCE@CB3Ph6** (orange). (c) Representation of the guest removal and encapsulation processes. The molecular packing of **CB3Ph6**α was depicted in detail as far as experimentally revealed. Gray rods, pink-filled circles, and green-dotted circles represent biphenyl units, *o*-carborane units, and vacant channels, respectively.

for SCXRD analysis could not be obtained. The crystal structure of **CB3Ph6α** was then examined using powder X-ray diffraction (PXRD) analysis (Fig. S3 and S4). Initially, the PXRD peak positions of **CB3Ph6α** were almost coincident with those of **DCE@CB3Ph6**, suggesting that they should have similar molecular packing. Moreover, the index assignment of the PXRD patterns revealed that **CB3Ph6α** has the same space group (*C*2/*c*) as **DCE@CB3Ph6**, with only slight changes in the crystal lattice upon guest removal. These results indicate that the crystalline molecular arrangement of **CB3Ph6α** can be preserved during the guest-removal process. From these facts, we presumed that **CB3Ph6α** might form unfilled channels in which guest molecules could be accommodated. To examine the validity of this assumption, the N_2 adsorption isotherm of **CB3Ph6α** was collected (Fig. 3a). It was found that **CB3Ph6α** had a typical type-I N_2 isotherm, indicating the presence of microporosity. The specific surface area was calculated to be 1.5×10^2 $m^2\ g^{-1}$ (Fig. S8), which was on the same order of magnitude as a porous crystal based on triangle compounds.[18] These results indicate that **CB3Ph6α** has permanent intrinsic porosity and maintains crystalline molecular alignment even after the removal of guest molecules.[18] Furthermore, adsorption isotherms were collected for CO_2, methane (CH_4), ethane (C_2H_6), butane (C_4H_{10}), and *n*-hexane (C_6H_{14}) (Fig. S9 and Table 1). **CB3Ph6α** showed the highest adsorption capability toward C_4H_{10}, which has multiple C–H moieties and the most similar molecular size to DCE among the tested gases. Therefore, guests with a C4 chain length should show optimal size matching with the cavity. The decrease in the adsorption capacity on C_6H_{14} is likely due to the size incompatibility, leading to the ineffective formation of C–H···π contacts between the host and guest molecules. Consequently, the adsorption data suggest that **CB3Ph6α** can capture vaporous guests of C4-length *via* C–H···π interactions.

The guest encapsulation of **CB3Ph6α** was studied by solid–vapor adsorption experiments. A crystalline sample of **CB3Ph6α** was exposed to the vapor of 1,2-dibromoethane (DBE) or 1-bromo-2-chloroethane (BCE), which have a similar molecular size to DCE, to prepare guest-loaded crystals (**DBE@CB3Ph6** or **BCE@CB3Ph6**, respectively). ^{1}H NMR spectra indicated that 1 : 1 encapsulation of the solvent molecules proceeded in both **DBE@CB3Ph6** and **BCE@CB3Ph6** (Charts S5, S6 and Table S2). The PXRD patterns of **DBE@CB3Ph6** and **BCE@CB3Ph6** were almost identical to those of **DCE@CB3Ph6** and **CB3Ph6α** (Fig. S4), indicating that the crystal-state arrangement of **CB3Ph6** should be hardly changed upon the adsorption of DBE or BCE. The re-uptake of DCE on **CB3Ph6α** was also monitored by PXRD and ^{1}H NMR measurements (Fig. S5 and Chart S7). The resulting crystals were evaluated using thermogravimetric analysis (TGA) (Fig. 3b and S10). The solvated crystals showed 10–20% weight loss between 100–200 °C, which was assignable to solvent release. The molar ratio of the included solvents to **CB3Ph6** was calculated to be 1 : 1 in the three solvated crystals, as observed *via* their ^{1}H NMR spectra (Table S2). The solvent release was also confirmed by endothermic peaks in differential scanning calorimetry thermograms (Fig. S11). In contrast, **CB3Ph6α** showed hardly any weight loss in the range of 100–200 °C, indicating complete removal of the guest solvents during activation. Reported porous organic compounds typically lose their porosity above approximately 100 °C,[23] with a maximum of ∼400 °C at best.[24] Notably, the decomposition temperature of the **CB3Ph6** crystal is over 500 °C, as calculated from TGA curves (Table S2), which highlights the robustness of the material owing to the inorganic 3D aromaticity of *o*-carborane scaffolds.[25,26] Moreover, in the variable-temperature PXRD measurement, the PXRD pattern of the crystal hardly changed up to at least 400 °C, indicating the superior heat resistance of the porous crystal without decomposition or melting (Fig. S12).

To evaluate the stability of the crystal, the non-covalent interaction (NCI) plot[27] was prepared to visualize intra- and inter-column interaction in the 1D **CB3Ph6** array formed in the crystal (Fig. S13). The NCI plot indicated that vdW interactions existed between the *o*-carborane units in the crystal, and other interactions such as B–H···π and C–H···H–B were also visualized, as indicated by the SCXRD data based on interatomic distances (Fig. S1 and S2). Therefore, at this stage, these data suggest that multiple non-covalent interactions cooperatively contribute to the reinforcement of the porous structure and its thermal stability.

Furthermore, the PXRD patterns confirmed their high crystallinity, as indicated by consistent peaks even after guest removal and refilling (Fig. S4). These data suggest that the rigid microporosity should be hardly affected by the desorption and adsorption processes. This high crystallinity enabled SCXRD analysis on **DBE@CB3Ph6** (Table S1 and Fig. S2). As we expected, **DBE@CB3Ph6** had the same crystalline packing as **DCE@CB3Ph6** except for the replacement of the halogen atoms. Its space group was determined to be *C*2/*c*, which is the same as that of **DCE@CB3Ph6** and **CB3Ph6α**. The differences between the lattice constants of the two crystals were less than 1%. From these results, it can be concluded that the removal and re-uptake of the vaporous guests proceed without crystal phase transition, amorphization or chemical decomposition (Fig. 3c). The solid–gas adsorption experiment of **CB3Ph6α** with C_4H_{10} was also carried out to investigate the guest selectivity. The adsorbed C_4H_{10} molecules were quantified using ^{1}H NMR measurements. After 30 min and 2 days of the adsorption experiment, the guest/host molar ratio was calculated to be 0.49 and 0.13, respectively (Charts S8 and S9). With DCE, DBE, and BCE, 1 : 1 host–guest binding was maintained for at least 30 min after the solid–vapor adsorption experiments (Charts S5–S7).

Table 1 Summary of the adsorption capacities of CB3Ph6α

Adsorbate	V/cm^3 (STP) per g at 298 K
CO_2	22.8[a]
CH_4	10.8[a]
C_2H_6	25.2[a]
C_4H_{10}	27.3[a]
C_6H_{14}	19.8[b]

[a] Measured under 100.4 kPa. [b] Measured under 18.3 kPa (saturated).

These results indicate that **CB3Ph6α** can capture gaseous C_4H_{10}, while its host–guest binding with C_4H_{10} could be weaker than that with halogenated ethane derivatives. Thus, it is presumed that the halogen atoms might render the C–H bonds more electron-deficient, which in turn enhances the C–H···π interactions with the biphenyl units.

Optical properties

Optical measurements were conducted to understand the effect of macrocyclization and host–guest complexation in the crystalline state on excited-state relaxation processes. **CB3Ph6** showed only slight photoluminescence (PL) in the $CHCl_3$ solution (emission quantum yield (Φ_{PL}) < 0.01), while crystalline samples exhibited values over 10 times larger (Φ_{PL} > 0.10) (Tables 2 and S3). Moreover, **CB3Ph6** exhibited emission enhancement by aggregation in the THF/H_2O mixture, in which THF and H_2O behaved as good and poor solvents, respectively (Fig. S14). These results indicate that **CB3Ph6** is an AIEgen. The absorption spectra were hardly influenced by solvent polarity, whereas the PL spectra were significantly red-shifted as the polarity increased (Fig. S15), meaning that the emission bands should be obtained from the ICT state in the solution state. As observed in the solution state, the crystalline samples showed structureless PL bands, indicating that the crystals should show ICT emission. These results suggested that in the excited state, macrocyclic **CB3Ph6** should have a significant relaxation pathway that is permissible even under structural constraints. Next, the effect of guest encapsulation was investigated for **CB3Ph6** crystals (Fig. 4a and Table 2). The correspondence between the PXRD patterns for the experimental and SCXRD simulated data (Fig. S6 and S7) confirmed the phase purity of the solvated crystals. The guest-free crystal, **CB3Ph6α**, showed a PL band with a maximum wavelength (λ_{PL}) of 461 nm and a Φ_{PL} of 0.11. Host–guest complexation in the solvated crystals resulted in a 14–23% increase of Φ_{PL} and a 4–12 nm blue-shift of λ_{PL}. The PL spectra of the solvated crystals completely overlapped each other, suggesting that the luminescence properties should be obtained through a similar mechanism despite the uptake of different guests. Reversible guest encapsulation was also confirmed by the correspondence between the PL spectra of **CB3Ph6α** exposed to DCE vapor (**DCE-fumed**) and **DCE@CB3Ph6** (Fig. 4b) and re-enhancement of the Φ_{PL} value to 0.33 in **DCE-fumed**. To gather kinetic information, the radiative and non-radiative constants (k_r and k_{nr}, respectively) were calculated using Φ_{PL} and lifetime data (Table 2 and Fig. S16, S17). It was revealed that the k_r values were hardly affected by solvent encapsulation, while the k_{nr} values decreased by an order of magnitude. This result suggests that guest molecules should inhibit non-radiative decay processes. It is widely known

Table 2 Summary of solid-state optical properties

Crystal	$\lambda_{PL}{}^{a}$/nm	$\Phi_{PL}{}^{a,b}$	$\tau_{PL}{}^{c}$/ns	τ_{PL}^{aved}/ns	χ^2	$k_r{}^{e}$/ns^{-1}	$k_{nr}{}^{f}$/ns^{-1}
CB3Ph6α	461	0.11	2.8 (51%), 0.9 (38%), 0.07 (11%)	0.5	1.22	0.22	1.8
DCE@CB3Ph6	456	0.29	2.6 (17%), 1.5 (79%), 0.1 (4%)	1.1	1.06	0.26	0.65
DBE@CB3Ph6	457	0.25	2.6 (19%), 1.2 (76%), 0.1 (4%)	0.9	1.09	0.28	0.83
BCE@CB3Ph6	454	0.34	2.4 (14%), 1.3 (83%), 0.1 (3%)	1.1	0.99	0.28	0.63

[a] Excited at 276 nm. [b] Absolute quantum yield determined by the integrating sphere method. [c] Excited at 375 nm. [d] $\tau_{PL}^{ave} = \sum_i \tau_i f_i$, where f_i: relative amplitude of the ith component (%), τ_i: luminescent decay lifetime of the ith component(s). [e] $k_r = \Phi_{PL}/\tau_{PL}^{ave}$. [f] $k_{nr} = (1 - \Phi_{PL})/\tau_{PL}^{ave}$.

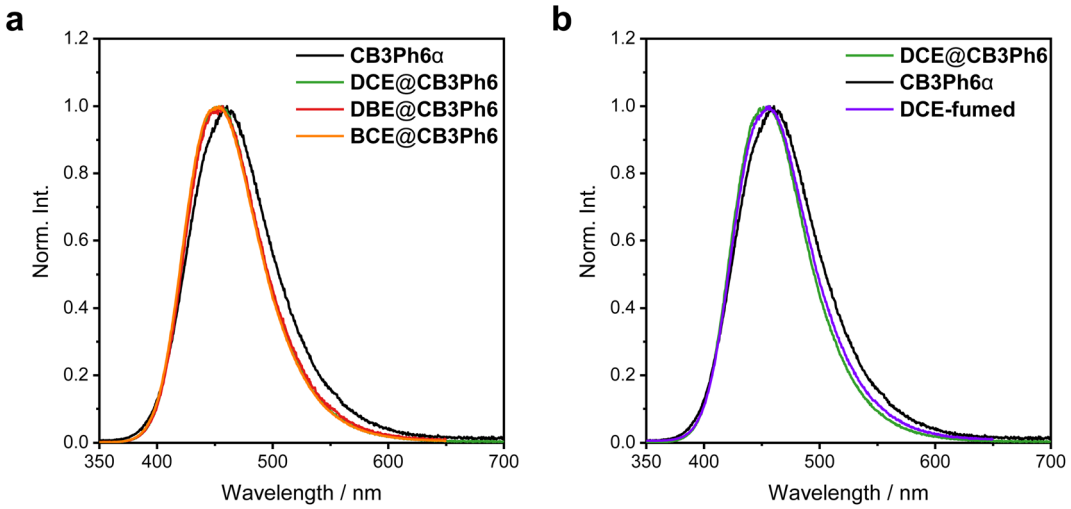

Fig. 4 (a) PL spectra of **CB3Ph6α** (black), **DCE@CB3Ph6** (green), **DBE@CB3Ph6** (red), and **BCE@CB3Ph6** (orange). (b) PL spectra of **DCE@CB3Ph6** before (green) and after (**CB3Ph6α**, black) the removal of vaporous guests and after re-uptake of DCE (**DCE-fumed**).

that cryogenic temperatures can suppress molecular motion that leads to non-radiative emission quenching. For the **CB3Ph6** crystals, cooling from room temperature to 77 K induced a blue-shift of the PL spectra by 15–17 nm (Fig. S18) and significant emission enhancement regardless of the presence of guest solvents in the crystal packing (Fig. S19). These cryogenic results corresponded to the phenomena observed upon solvent encapsulation, which further implies that the included guest solvents should block the molecular motions that cause emission quenching.

DFT calculations

To understand the mechanism behind the guest-induced emission enhancement, theoretical calculations were performed using density functional theory (DFT) and time-dependent DFT (TD-DFT). DFT calculations for the ground state show that the calculated structure is identical to the SCXRD structure (Fig. 2a), and that isolated **CB3Ph6** should have a C_3-symmetry with an equal length of the C_{cage}–C_{cage} bonds in three *o*-carborane units (1.75 Å) and vertically oriented biphenyl sides to the C_{cage}–C_{cage} bonds (Fig. 5 left and S20a). The absorption transition (S_0 to S_1) involved molecular orbitals (MOs) contributed by biphenyl units (Fig. S21). TD-DFT calculations for the excited state suggest a locally-stable geometry with the C_{cage}–C_{cage} bond elongated to 2.36 Å (Fig. 5 middle and S20b). The emission transition (S_1 to S_0) was calculated as the ICT character between the lowest unoccupied MO (LUMO) and the highest occupied MO (HOMO). The HOMO contains the π* orbitals of two biphenyl units, while the LUMO mainly extends over the *o*-carborane unit (Fig. 5 middle). These results support that **CB3Ph6** exhibits ICT emission contributed by one *o*-carborane unit and two biphenyl units connected to it.

To understand the guest-induced PL change, crystal-state calculations were performed with the quantum mechanics and molecular mechanics (QM/MM) method.[28] The QM/MM calculation was modeled using a cut out cluster of the SCXRD packing structures (Fig. S22). The model structure for the guest-free crystal, **CB3Ph6α**, was prepared based on solvent-removed **DCE@CB3Ph6**. From the calculations, it was proposed that guest encapsulation of DCE and DBE can induce 4 and 6 nm blue shifts of the PL spectra, respectively. These results are in close agreement with the experimental data, with blue shifts of up to 7 nm being observed (Table S4). In addition, guest encapsulation slightly suppressed C_{cage}–C_{cage} bond elongation (Fig. S23a–c). It is implied that structural relaxation in the excited state, followed by the PL blue-shift, might be caused by the limited structural relaxation. Furthermore, in the non-emissive dark excited states, the distributions of the HOMO and LUMO were almost separate (Fig. 5 right). As a result, the corresponding emission transitions are forbidden and show almost no oscillator strength, owing to only slight overlap between the HOMO and LUMO distributions (Table S17). In the dark state, isolated **CB3Ph6** had a C_{cage}–C_{cage} bond length of 2.49 Å and one biphenyl unit oriented parallel to the elongated bond (Fig. 5 right and S20c). The rotated biphenyl moiety partially filled the internal cavities of **CB3Ph6**. The crystalline dark states were also found from the calculations using the QM/MM method (Fig. S23d–f). The dark state of **CB3Ph6α** was destabilized by 0.19 eV as compared to the corresponding ICT

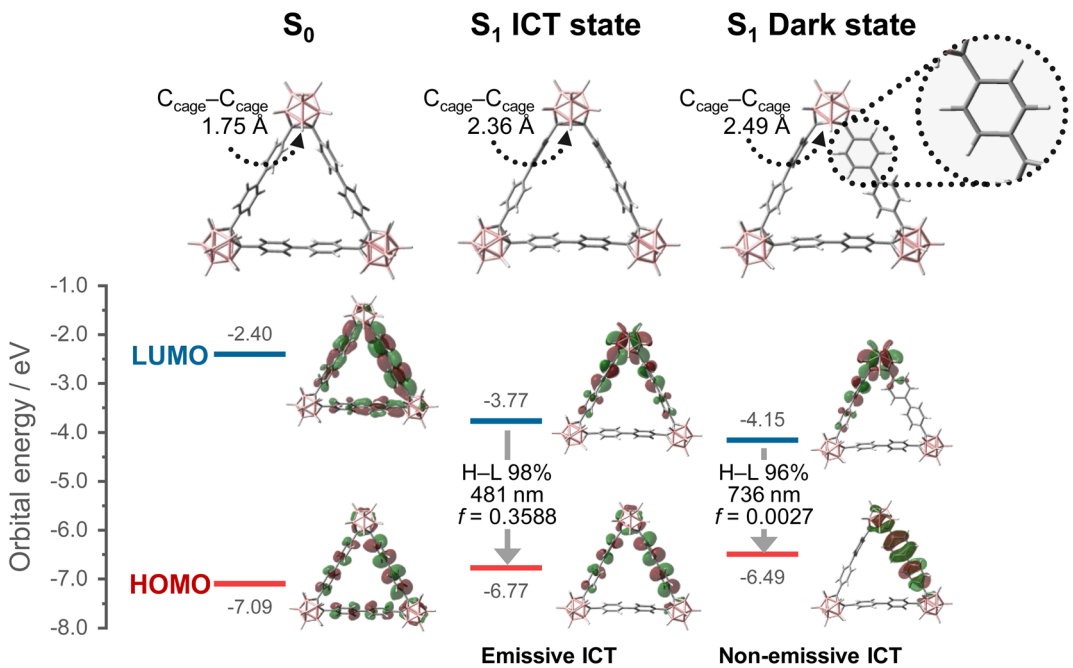

Fig. 5 Optimized structures with the C_{cage}–C_{cage} bond lengths and calculated Kohn–Sham frontier orbital distributions of the S_0 (left), S_1 ICT (middle), and S_1 dark states (right) of **CB3Ph6**, with the electronic transition energy in nm and the assigned emission characters for the S_1 states (colors: C, gray; B, pink; H, white). H–L indicates the proportion of HOMO–LUMO transitions consisting of the $S_1 \rightarrow S_0$ transition. *f* denotes the oscillator strength. Isovalues are 0.02. B3LYP/6-31+G(d,p) was used. Red and blue bar plots indicate HOMO and LUMO energy levels, respectively.

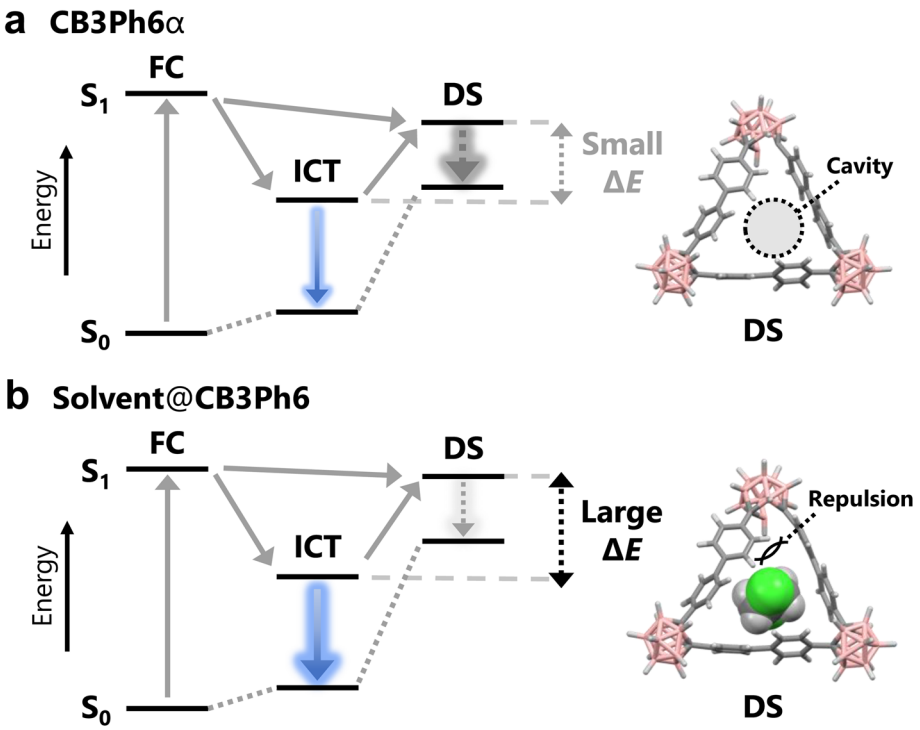

Fig. 6 Schematic illustration of the energy diagrams of (a) **CB3Ph6**α and (b) guest-encapsulated **CB3Ph6** crystals with the corresponding QM-calculated molecular structure of the dark states (colors: C, gray; B, pink; H, white; Cl, green), in which the solvent is DCE, DBE, or BCE. FC, ICT, and DS denote Franck–Condon, intramolecular charge transfer, and dark states, respectively. Blue solid and gray dotted arrows indicate transitions dominated by radiative and non-radiative decay, respectively.

state. Significantly, the degree of destabilization was enlarged by guest encapsulation; the energy levels of the dark states of DCE and DBE in the crystal should be 0.38 and 0.44 eV higher than those of their ICT states, respectively (Table S5). In other systems, it has been reported that guest-induced PL changes are related to the suppression of structural changes in the excited state.[29] In this case, the experimentally observed guest-induced emission enhancement of **CB3Ph6** was associated with the decreased non-radiative decay constants, possibly due to the suppression of excited-state structural relaxation. Assuming ultrafast decay in the dark state, these results suggest the possibility that, in the absence of guest-loading, the benzene rings can rotate smoothly in the cavity, which accelerates relaxation to the non-emissive dark state, while guest filling could partially disturb the formation of dark states *via* steric repulsion. This should then facilitate the trapping of more excitons in the emissive ICT states. Finally, emission enhancements could be induced by guest encapsulation (Fig. 6).

Conclusion

In conclusion, we have shown that **CB3Ph6**, a novel AIE-active *o*-carborane-based macrocycle, can form a permanent intrinsic porous crystal with 1D channels. Solid–vapor adsorption indicated that vaporous halogenated ethane derivatives can thread into the channel to construct a 1 : 1 host–guest complex. The crystal can be processed with reversible guest removal and encapsulation without losing its porosity and crystallinity. Vapor inclusion induced a blue-shift and the enhancement of PL efficiency. Theoretical calculation data suggest that filling of the cavity by vaporous guests could restrict excited-state structural relaxation in the crystal state. Furthermore, the porous crystal has excellent thermal stability up to 500 °C. One possible application of our material is the separation and detection of alkanes and alkynes based on whether multiple effective C–H$\cdots\pi$ interactions can be formed. Our findings might contribute to the expansion of the design and application of smart materials based on porous molecular crystals utilizing AIEgens.

Author contributions

K. Y., S. T., T. Y., and S. O. performed experiments and conducted data analysis. K. Y. conducted investigation and wrote the original draft. K. Y. and K. T. conceptualized the research framework. T. O. and K. T. provided resources and supervised the project. All authors discussed the results and contributed to reviewing and editing the manuscript.

Conflicts of interest

There are no conflicts to declare.

Data availability

The data supporting this article have been included as part of the supplementary information (SI). Supplementary information is available. See DOI: https://doi.org/10.1039/d5sc08753h.

CCDC 2495493 (**DCE@CB3Ph6**) and 2495494 (**DBE@CB3Ph6**) contain the supplementary crystallographic data for this paper.[30a,b]

Acknowledgements

This work was partially supported by a Grant-in-Aid for Scientific Research (B) (for K. T., JSPS KAKENHI Grant Number, 24K01570) and the National Research Foundation of Korea (NRF) grant funded by the Korea government (MSIT) (No. RS-2024-00406152).

References

1 M. K. Bera, P. Pal and S. Malik, Solid-state emissive organic chromophores: design, strategy and building blocks, *J. Mater. Chem. C*, 2020, **8**, 788–802.
2 J. Mei, Y. Hong, J. W. Y. Lam, A. Qin, Y. Tang and B. Z. Tang, Aggregation-induced emission: the whole is more brilliant than the parts, *Adv. Mater.*, 2014, **26**, 5429–5479.
3 Y. Cai, L. Du, K. Samedov, X. Gu, F. Qi, H. H. Y. Sung, B. O. Patrick, Z. Yan, X. Jiang, H. Zhang, J. W. Y. Lam, I. D. Williams, D. Lee Phillips, A. Qin and B. Z. Tang, Deciphering the working mechanism of aggregation-induced emission of tetraphenylethylene derivatives by ultrafast spectroscopy, *Chem. Sci.*, 2018, **9**, 4662–4670.
4 Y. Fujimoto, Y. Mochiduki, H. Sotome, R. Shimada, H. Okajima, Y. Toda, A. Sakamoto, H. Miyasaka and F. Ito, Excited State Dynamics of Geometrical Evolution of α-Substituted Dibenzoylmethanatoboron Difluoride Complex with Aggregation-Induced Emission Property, *J. Am. Chem. Soc.*, 2024, **146**, 32529–32538.
5 Z. Jianyu, Z. Haoke, L. W. Jacky Y and T. Ben Zhong, Restriction of Intramolecular Motion (RIM): Investigating AIE Mechanism from Experimental and Theoretical Studies, *Chem. Res. Chin. Univ.*, 2021, **37**, 1–15.
6 Y. Duo, L. Han, Y. Yang, Z. Wang, L. Wang, J. Chen, Z. Xiang, J. Yoon, G. Luo and B. Z. Tang, Aggregation-Induced Emission Luminogen: Role in Biopsy for Precision Medicine, *Chem. Rev.*, 2024, **124**, 11242–11347.
7 Y. Huang, L. Ning, X. Zhang, Q. Zhou, Q. Gong and Q. Zhang, Stimuli-fluorochromic smart organic materials, *Chem. Soc. Rev.*, 2024, **53**, 1090–1166.
8 K. Imato and Y. Ooyama, Stimuli-responsive smart polymers based on functional dyes, *Polym. J.*, 2024, **56**, 1093–1109.
9 J. R. Wu, G. Wu, D. Li and Y. W. Yang, Macrocycle-Based Crystalline Supramolecular Assemblies Built with Intermolecular Charge-Transfer Interactions, *Angew. Chem., Int. Ed.*, 2023, **62**, e202218142.
10 A. Liu and Y. W. Yang, Aggregation-induced emission in synthetic macrocycle-based supramolecular systems, *Chem. Commun.*, 2025, **61**, 13827–13840.
11 J. Ochi, K. Tanaka and Y. Chujo, Recent Progress in the Development of Solid-State Luminescent o-Carboranes with Stimuli Responsivity, *Angew. Chem., Int. Ed.*, 2020, **59**, 9841–9855.
12 L. A. Boyd, W. Clegg, R. C. B. Copley, M. G. Davidson, M. A. Fox, T. G. Hibbert, J. A. K. Howard, A. Mackinnon, R. J. Peace and K. Wade, Exo-π-bonding to an ortho-carborane hypercarbon atom: systematic icosahedral cage distortions reflected in the structures of the fluoro-, hydroxy- and amino-carboranes, 1-X-2-Ph-1,2-$C_2B_{10}H_{10}$ (X = F, OH or NH_2) and related anions, *Dalton Trans.*, 2004, 2786–2799.
13 H. Naito, K. Nishino, Y. Morisaki, K. Tanaka and Y. Chujo, Solid-State Emission of the Anthracene-o-Carborane Dyad from the Twisted-Intramolecular Charge Transfer in the Crystalline State, *Angew. Chem., Int. Ed.*, 2017, **56**, 254–259.
14 D. Tahaoğ Lu, H. Usta and F. Alkan, Revisiting the Role of Charge Transfer in the Emission Properties of Carborane–Fluorophore Systems: A TDDFT Investigation, *J. Phys. Chem. A*, 2022, **126**, 4199–4210.
15 L. Ji, S. Riese, A. Schmiedel, M. Holzapfel, M. Fest, J. Nitsch, B. F. E. Curchod, A. Friedrich, L. Wu, H. H. Al Mamari, S. Hammer, J. Pflaum, M. A. Fox, D. J. Tozer, M. Finze, C. Lambert and T. B. Marder, Thermodynamic equilibrium between locally excited and charge-transfer states through thermally activated charge transfer in 1-(pyren-2′-yl)-o-carborane, *Chem. Sci.*, 2022, **13**, 5205–5219.
16 M. Tokutomi, K. Yuhara and K. Tanaka, Macrocyclic C,C′-diaryl-o-carborane derivatives containing pseudo-crown ether: emission enhancement upon cation recognition, *Phys. Chem. Chem. Phys.*, 2025, **27**, 15845–15849.
17 Y. Wang, H. Wu and J. F. Stoddart, Molecular Triangles: A New Class of Macrocycles, *Acc. Chem. Res.*, 2021, **54**, 2027–2039.
18 A. Chaix, G. Mouchaham, A. Shkurenko, P. Hoang, B. Moosa, P. M. Bhatt, K. Adil, K. N. Salama, M. Eddaoudi and N. M. Khashab, Trianglamine-Based Supramolecular Organic Framework with Permanent Intrinsic Porosity and Tunable Selectivity, *J. Am. Chem. Soc.*, 2018, **140**, 14571–14575.
19 Q. Qu, M. Fu, C. Lin, Y. Geng, Y. Li and Y. Yuan, Synthesis, properties and application of o-carborane-based π-conjugated macrocycles, *Org. Chem. Front.*, 2023, **10**, 3293–3299.
20 W. Jiang, I. T. Chizhevsky, M. D. Mortimer, W. Chen, C. B. Knobler, S. E. Johnson, F. A. Gomez and M. F. Hawthorne, Carboracycles: Macrocyclic Compounds Composed of Carborane Icosahedra Linked by Organic Bridging Groups, *Inorg. Chem.*, 1996, **35**, 5417–5426.
21 M. Mastalerz, Permanent porous materials from discrete organic molecules-towards ultra-high surface areas, *Chem.–Eur. J.*, 2012, **18**, 10082–10091.
22 S. Cheng, L. Zong, K. Yuan, J. Han, X. Jian and J. Wang, Synthesis and thermal properties of an acetylenic monomer containing boron and silicon, *RSC Adv.*, 2016, **6**, 88403–88410.
23 H. Yamagishi, Functions and fundamentals of porous molecular crystals sustained by labile bonds, *Chem. Commun.*, 2022, **58**, 11887–11897.
24 C. G. Bezzu, L. A. Burt, C. J. McMonagle, S. A. Moggach, B. M. Kariuki, D. R. Allan, M. Warren and N. B. McKeown,

Highly stable fullerene-based porous molecular crystals with open metal sites, *Nat. Mater.*, 2019, **18**, 740–745.

25 A. Muñoz-Castro, Aromatic trails: persistence and interplay between linked spherical aromatic dicarboranes in dimer to hexamer linear arrays, *Phys. Chem. Chem. Phys.*, 2025, **27**, 5249–5255.

26 P. L. Rodríguez-Kessler and A. Muñoz-Castro, Macrocyclic meta-carborane hexamer. Evaluation of aromatic characteristics as a cluster-based analog to phenyl-bridged macrocyclic structures, *Phys. Chem. Chem. Phys.*, 2025, **27**, 6744–6750.

27 E. R. Johnson, S. Keinan, P. Mori-Sánchez, J. Contreras-García, A. J. Cohen and W. Yang, Revealing noncovalent interactions, *J. Am. Chem. Soc.*, 2010, **132**, 6498–6506.

28 Q. Wu, T. Zhang, Q. Peng, D. Wang and Z. Shuai, Aggregation induced blue-shifted emission-the molecular picture from a QM/MM study, *Phys. Chem. Chem. Phys.*, 2014, **16**, 5545–5552.

29 M. Rojas-Poblete, P. L. Rodríguez-Kessler, R. Guajardo Maturana and A. Muñoz-Castro, Coinage-metal pillarplexes hosts. Insights into host-guest interaction nature and luminescence quenching effects, *Phys. Chem. Chem. Phys.*, 2021, **23**, 15917–15924.

30 (*a*) CCDC 2495493: Experimental Crystal Structure Determination, 2025, DOI: 10.5517/ccdc.csd.cc2prrs0; (*b*) CCDC 2495494: Experimental Crystal Structure Determination, 2025, DOI: 10.5517/ccdc.csd.cc2prrt1.